Ground Movements due to Shallow Tunnels in Soft Ground. I: Analytical Solutions

Federico Pinto[1] and Andrew J. Whittle, M.ASCE[2]

Abstract: This paper presents simplified closed-form analytical solutions that can be used to interpret and predict ground movements caused by shallow tunneling in soft ground conditions. These solutions offer a more comprehensive framework for understanding the distribution of ground movements than widely used empirical functions. Analytical solutions for the displacement field within the ground mass are obtained for two basic modes of deformation corresponding to uniform convergence and ovalization at the wall of a circular tunnel cavity, based on the assumption of linear, elastic soil behavior. Deformation fields based on the superposition of fundamental, singularity solutions are shown to differ only slightly from analyses that consider the physical dimensions of the tunnel cavity, except in the case of very shallow tunnels. This work demonstrates a simplified method to account for soil plasticity in the analyses and illustrate closed-form solutions for a three-dimensional (3D) tunnel heading. A companion paper describes applications of these analyses to interpret field measurements of ground response to tunneling. **DOI: 10.1061/(ASCE)GT.1943-5606.0000948.**

Author keywords: Tunnels; Ground loss; Elasticity; Soil stiffness; Plasticity; Deformation analysis.

Introduction

The prediction and mitigation of damage caused by construction-induced ground movements represents a major factor in the design of tunnels. This is an especially important problem for shallow tunnels excavated in soft soils, where expensive remedial measures such as compensation grouting or structural underpinning may need to be considered prior to construction.

Ground movements arise from changes in soil stresses around the tunnel face and the overexcavation of the final tunnel cavity, often referred to as ground loss. Sources of movements are closely related to the method of tunnel construction ranging from (1) closed-face systems such as tunnel boring machines (with earth pressure or slurry shields), where overcutting occurs around the face and shield (i.e., the tail void) while local ground loss is constrained by grout injected between the soil and precast lining system, to (2) open-face systems [e.g., New Austrian Tunneling Method (NATM)] where ground loss around the heading is controlled by expeditious installation of lining systems in contact with the soil (typically steel rib or lattice girder and shotcrete) with additional face support provided by a closed-shield or other mechanical reinforcement or improvement (soil nails, subhorizontal jet grouting, etc.). In all cases, it is easy to appreciate the complexity of the mechanisms causing ground movement and their close relationship with construction details, especially given the complex mechanical properties of soils, and their linkage to groundwater flows.

This complexity has encouraged the widespread use of numerical analyses, particularly nonlinear FEMs, over a period of more than 30 years (e.g., review by Gioda and Swoboda 1999). Although these powerful numerical analyses undoubtedly provide the most comprehensive framework for modeling tunneling processes and interactions with other existing structures (e.g., Potts and Addenbrooke 1997), their predictive accuracy is also closely tied to the knowledge of in situ conditions and the modeling of soil behavior.

Despite the extensive research and progress in numerical analyses, the prediction and interpretation of far-field ground movements is still largely based on empirical methods. The most extensive data relate to the transverse ground surface settlement trough for greenfield conditions. Following Peck (1969) and Schmidt (1969), the surface settlement for a circular tunnel of radius, R, is usually described by a Gaussian distribution function, Fig. 1

$$u_y(x, y = 0) = u_y^0 \exp\left(-\frac{x^2}{2x_i^2}\right) \tag{1}$$

where u_y^0 = centerline settlement above the crown; and x_i = inflection point in the curve. These parameters are fitted to field monitoring data. Data compiled by Mair and Taylor (1997) suggest average values, $x_i/H = 0.35$ and 0.50 for tunnels in sands and clays, respectively (H is the depth to the spring line of the tunnel, Fig. 1).

The displaced volume of the ground surface, $\Delta V_s = 2.5 u_y^0 x_i$ is often equated with the volume loss occurring at the tunnel cavity, ΔV_L (i.e., $\Delta V_g = 0$, Fig. 1). This appears to be a valid approximation for undrained shearing associated with the short term response of tunnels in clay.

In addition, a variety of analytical solutions have been proposed for estimating the two-dimensional (2D) distribution of ground movements for shallow tunnels in soft ground (notably Sagaseta 1987; Verruijt and Booker 1996; Verruijt 1997; González and Sagaseta 2001). These analyses make simplifying assumptions regarding the constitutive behavior of soil, but otherwise fulfill the principles of continuum mechanics. In principle, these analytical solutions provide a more consistent framework for interpreting horizontal and vertical components of ground deformations than conventional empirical models and use a small number of input parameters that can be readily calibrated to field data. They also provide a useful basis for evaluating the accuracy of numerical analyses.

This paper presents a detailed review and comparison of the analytical solutions for estimating far-field ground movements for shallow

[1]Associate Professor, FCEFyN Universidad Nacional de Córdoba - CONICET, Córdoba 5016, Argentina.

[2]Professor, Massachusetts Institute of Technology, Cambridge, MA 02139 (corresponding author). E-mail: ajwhittl@mit.edu

Note. This manuscript was submitted on August 16, 2011; approved on April 9, 2013; published online on May 30, 2013. Discussion period open until May 3, 2014; separate discussions must be submitted for individual papers. This paper is part of the ***Journal of Geotechnical and Geoenvironmental Engineering***, © ASCE, ISSN 1090-0241/04013040(17)/$25.00.

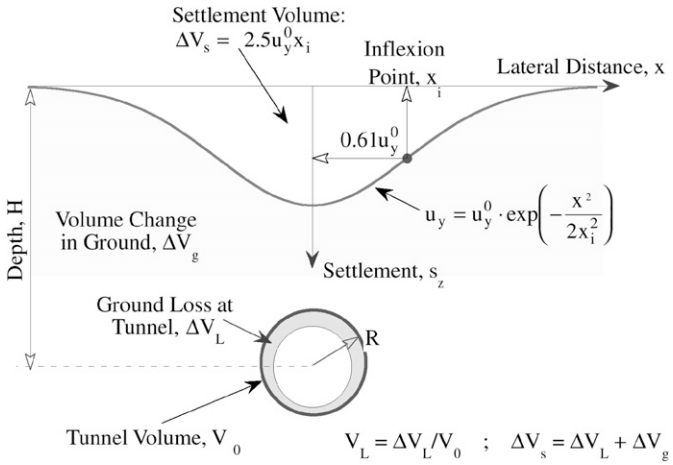

Fig. 1. Empirical function for transversal surface settlement trough (adapted from Peck 1969)

tunnels. This work presents some extensions of the published solutions and illustrates further application for a three-dimensional (3D) tunnel heading. A companion paper describes the practical application and interpretation of the analyses using field data (Pinto et al. 2013).

Deep Tunnel in Elastic Soil

The development of a rigorous analytical solution for shallow tunnels is complicated by the geostatic gradient of in situ stresses and by the traction-free boundary conditions at the ground surface (and potentially by other factors such as hydraulic gradients resulting from seepage, etc.). To avoid these difficulties, the first case chosen is that of a deep circular tunnel in an elastic soil, a problem first solved by Kirsch (1898). The in situ, in-plane stress state at the spring line can be decomposed into volumetric and deviatoric total stress components

$$p_0 = \sigma'_{v0}\frac{(1+K_0)}{2} + p_w \tag{2a}$$

$$q_0 = \sigma'_{v0}\frac{(1-K_0)}{2} \tag{2b}$$

where σ'_{v0} = initial vertical effective stress (the paper adopts the standard continuum mechanics convention with stresses and pore pressures positive in tension); K_0 = coefficient of earth pressures at rest; and p_w = pore pressure.

Assuming the soil is isotropic and linear, changes in the volumetric stress will produce a uniform convergence of the tunnel cavity, u_ε, while changes in the deviatoric stress will produce an ovalization, u_δ, as defined in Fig. 2. The deformations (u_x, u_y) in the surrounding soil caused by reducing stresses in the tunnel cavity can be written as follows:

$$\text{Convergence: } \begin{cases} u_x(x,y) = u_\varepsilon \dfrac{xR}{x^2+y^2} \\ u_y(x,y) = u_\varepsilon \dfrac{yR}{x^2+y^2} \end{cases} \tag{3a}$$

$$\text{Ovalization: } \begin{cases} u_x(x,y) = u_\delta \dfrac{R}{3-4\nu} x \dfrac{(3-4\nu)\left(x^2+y^2\right)^2 - \left(3y^2-x^2\right)\left(x^2+y^2-R^2\right)}{\left(x^2+y^2\right)^3} \\ u_y(x,y) = -u_\delta \dfrac{R}{3-4\nu} y \dfrac{(3-4\nu)\left(x^2+y^2\right)^2 - \left(3x^2-y^2\right)\left(x^2+y^2-R^2\right)}{\left(x^2+y^2\right)^3} \end{cases} \tag{3b}$$

where R = tunnel radius; ν = elastic Poisson ratio; and u_ε, u_δ = deformations occurring at the tunnel cavity.

Eq. (3*b*) can be further simplified [ignoring terms $O(R/r)^3$] if the displacements are to be evaluated in the far field

$$\text{Ovalization(far-field approximation): } \begin{cases} u_x(x,y) = u_\delta \dfrac{4(1-\nu)}{3-4\nu} R \dfrac{x\left(x^2 - \dfrac{\nu}{1-\nu}y^2\right)}{\left(x^2+y^2\right)^2} \\ u_y(x,y) = u_\delta \dfrac{4(1-\nu)}{3-4\nu} R \dfrac{y\left(\dfrac{\nu}{1-\nu}x^2 - y^2\right)}{\left(x^2+y^2\right)^2} \end{cases} \tag{3c}$$

In subsequent sections, the cavity wall displacements are considered as input parameters that define the distribution of ground movements. However, it is also interesting to consider the ideal case where there is no shear traction at the tunnel cavity, and an interior pressure, p_i (e.g., resulting from pressurized grouting or simple compression of the lining ring). In this case, the maximum elastic wall deflections are

$$\begin{aligned} u_\varepsilon &= \frac{(p_0 - p_i)R}{2G} \\ u_\delta &= -\frac{q_0 R}{2G}(3-4\nu) \end{aligned} \tag{4a}$$

where G = shear modulus of the soil. The relative distortion of the cavity, ρ, can then be found as (Sagaseta 1998)

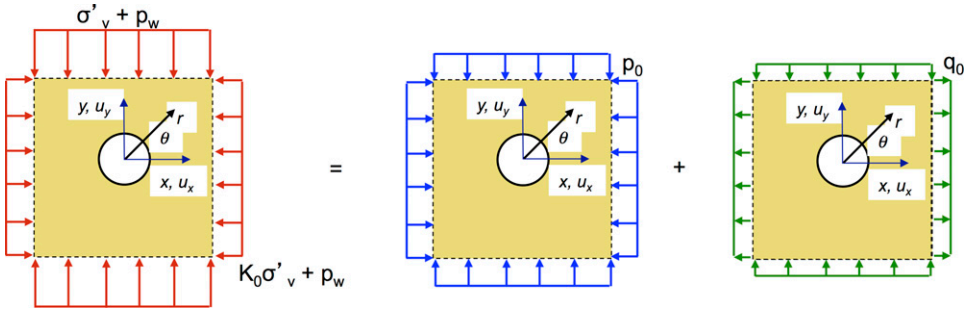

Fig. 2. Decomposition of initial stresses around deep tunnel

$$\rho = -\frac{u_\delta}{u_\varepsilon} = \frac{1-K_0}{1+K_0+2r_u}\frac{3-4\nu}{1-p_r} \tag{4b}$$

where $r_u = p_w/\sigma'_{V0}$ = pore pressure ratio; and $p_r = p_i/p_0$ = total pressure ratio.

Although this result corresponds to an idealized boundary condition for a deep tunnel, it provides a useful benchmark for interpreting the factors affecting the relative distortion parameter. Fig. 3 illustrates the influence of the parameters ν, K_0, and r_u on the expected range of ρ. The results show that $\rho > 0$ for all situations with $K_0 < 1.0$. Lower values of Poisson's ratio produce higher relative distortions (i.e., small values of ν amplify the distortion mode). In principle, $\rho < -1$ (i.e., upward displacement of tunnel crown) can occur for combinations of large K_0 and small ν.

Shallow Tunnel

Fig. 4 shows the notation and sign convention used in the analysis of a shallow circular tunnel with spring line located at a depth $y = H$ below the stress-free ground surface. The deformations of the tunnel cavity can now be decomposed into three basic modes: (1) uniform convergence, u_ε; (2) ovalization, u_δ (with no net change in volume of the cavity); and (3) vertical translation, Δu_y (buoyancy effect). The convergence component u_ε is clearly related to the change in volume of the tunnel cavity (per unit length), $2u_\varepsilon/R = \Delta V_L/V_0$, where ΔV_L is the ground loss and V_0 is the initial tunnel volume (cf. Fig. 1). There are two methods that have been proposed for analyzing the shallow tunnel problem. The first is the approximate solution based on the superposition of singularity solutions [Eqs. (3*a*)–(3*c*); Sagaseta 1987; Verruijt and Booker 1996] that implicitly ignore the finite dimensions of the tunnel itself. A more analytically complete solution (referred to as the exact case) was introduced by Verruijt (1997) based on 2D functions of a complex variable. It should be noted that neither the approximate nor the exact solutions account directly for the buoyancy effects associated with geostatic stress gradients in the ground (or other more complex features of soil stratification, etc.). The following sections summarize and compare these two formulations.

Approximate Solution

Fig. 5 illustrates the superposition of singularity solutions used to represent deformations for a shallow tunnel. In the current derivation, the normal traction components on the ground surface (x, $y = 0$) are cancelled by superimposing the full-space singularity solutions [Eqs. (3*a*) and (3*b*) for convergence and ovalization modes, respectively] located at $x = 0$ and $y = H$, with negative mirror image solutions at $x = 0$ and $y = -H$. Boundary conditions for the ground surface are then satisfied by introducing a distribution of corrective shear tractions and computing the ground deformations they produce

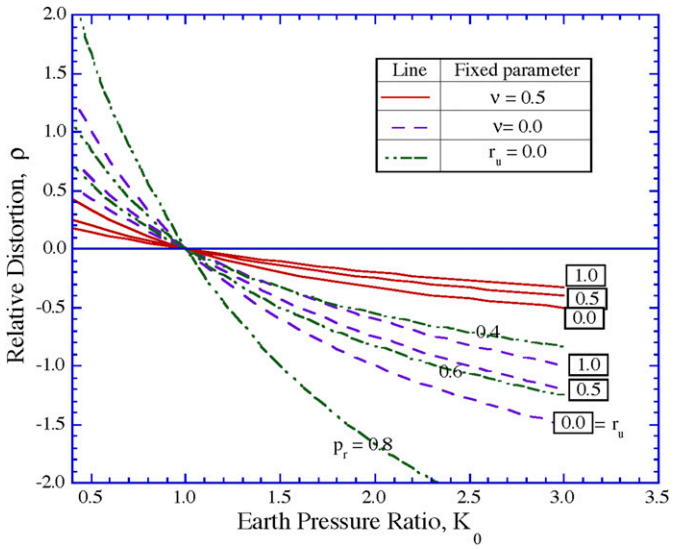

Fig. 3. Relative distortion values for deep tunnel cavity in elastic soil

$$\mathbf{u} = \mathbf{u}^\infty(x, y_1) - \mathbf{u}^\infty(x, y_2) + \mathbf{u}^c(x, y) \tag{5}$$

where $\mathbf{u}^\infty$ = deformation vector for the full-space solutions [Eqs. (3*a*) and (3*b*)]; $y_1 = (y + H)$; $y_2 = (y - H)$; and $\mathbf{u}^c$ = deformations that result from the corrective surface shear tractions.

Appendix I gives a brief account of the derivation of the corrective displacements, $\mathbf{u}^c$, from the singularity solutions for uniform convergence and ovalization. The results for the uniform convergence mode are as follows:

$$u_x^c = 4u_\varepsilon R\left\{\frac{(1-\nu)x}{x^2+(y-H)^2} - \frac{(y-H)xy}{\left[x^2+(y-H)^2\right]^2}\right\}$$

$$u_y^c = 2u_\varepsilon R\left\{\frac{2(y-H)x^2 + H\left[x^2-(y-H)^2\right]}{\left[x^2+(y-H)^2\right]^2} - \frac{2(1-\nu)(y-H)}{x^2+(y-H)^2}\right\} \tag{6a}$$

These solutions are identical to results presented by Verruijt and Booker (1996) using a different superposition method.

The current solutions for the ovalization mode (Pinto 1999) are based on corrective tractions from the complete singularity solutions for the line distortion [Eq. (3*b*)] as opposed to the far field approximations [i.e., Eq. (3*c*)] published previously

J. Geotech. Geoenviron. Eng. 2014.140.

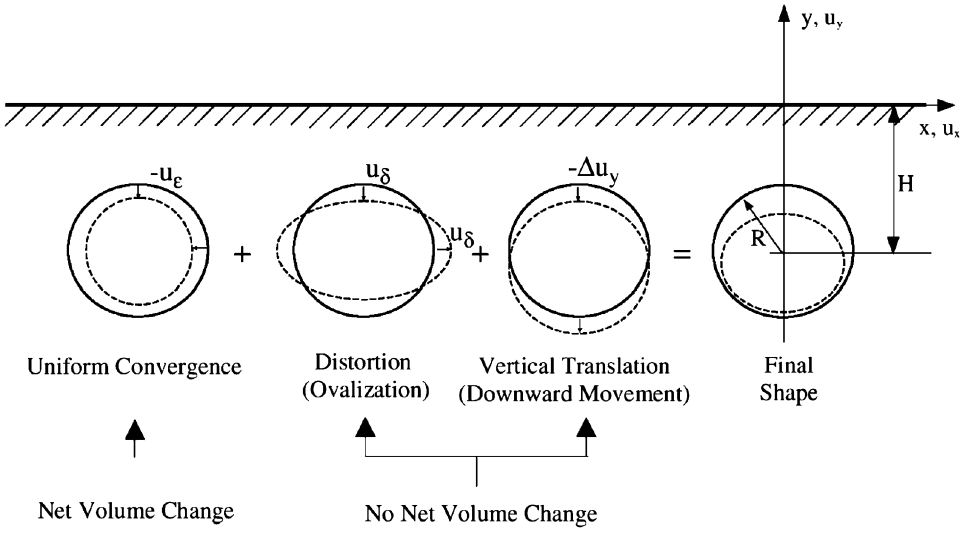

Fig. 4. Deformation modes and notation for shallow tunnel

$$u_x^c = \frac{8u_\delta R}{3-4\nu}\left\{ x\frac{x^2+y^2-H^2}{\left[x^2+(y-H)^2\right]^2}(1-\nu) - xy\frac{y\left(x^2+y^2\right)+2H\left(H^2-x^2\right)-3yH^2}{\left[x^2+(y-H)^2\right]^3}\right\} \tag{6b}$$

$$u_y^c = \frac{8u_\delta R}{3-4\nu}\left\{ \frac{x^2(2H-y)-y(y-H)^2}{\left[x^2+(y-H)^2\right]^2}(1-\nu) - \frac{(y-H)\left\{Hy(y-H)^2-x^2\left[\left(x^2+y^2\right)+H(y+H)\right]\right\}}{\left[x^2+(y-H)^2\right]^3}\right\} \tag{6c}$$

The superposition method generates (parasitic) vertical displacements for both the convergence and ovalization modes. The average vertical translation at the tunnel spring line is given by

$$\text{Convergence: } \frac{\Delta u_y}{u_\varepsilon} = 4\frac{R}{H}\frac{8(1-\nu)-(1-2\nu)\left(\frac{R}{H}\right)^2}{\left[4+\left(\frac{R}{H}\right)^2\right]^2}$$

$$\text{Ovalization: } \frac{\Delta u_y}{u_\delta} = \frac{2}{3-4\nu}\frac{R}{H}\frac{(1-8\nu)\left(\frac{R}{H}\right)^4+(11-8\nu)4\left(\frac{R}{H}\right)^2-32}{\left[4+\left(\frac{R}{H}\right)^2\right]^3} \tag{7}$$

Exact Solution

The solution method used by Verruijt (1997) is based on the complex formulation of planar elasticity. The complex formulation of planar elasticity is particularly suitable for this type of problem as it allows mapping the domain to describe both boundaries (i.e., tunnel wall and surface) by a single coordinate. In this formulation, the general solution of the equations is expressed in terms of two functions of complex variable (ϕ and ψ) called Goursat functions. These functions are found by imposing the displacement boundary conditions at the tunnel wall. The displacements are related to these functions as follows (e.g., Muskhelishvili 1963):

$$2Gu_z(z) = \kappa\phi(z) - z\overline{\frac{d\phi}{dz}} - \overline{\psi(z)} \tag{8a}$$

where $\kappa = (3-4\nu)$; G = elastic shear modulus; i = imaginary constant; ϕ and ψ = Goursat functions; overbar = complex conjugate; and

$$z = x + i\cdot y \tag{8b}$$

$$u_z = u_x + i\cdot u_y \tag{8c}$$

The original domain (z-space) is mapped onto an annular region on the auxiliary domain (ζ-space) by the following conformal transformation:

$$\zeta(z) = \frac{i\cdot z\cdot\left(1+\alpha^2\right)-H\cdot\left(1-\alpha^2\right)}{i\cdot z\cdot\left(1+\alpha^2\right)+H\cdot\left(1-\alpha^2\right)} \tag{9a}$$

where α is given by

$$\alpha = \frac{H}{R} - \sqrt{\left(\frac{H}{R}\right)^2-1} \tag{9b}$$

In this transformation, the ground surface ($y=0$, z-space) is mapped onto a circle of unit radius in the ζ-space, Fig. 6, and the

J. Geotech. Geoenviron. Eng. 2014.140.

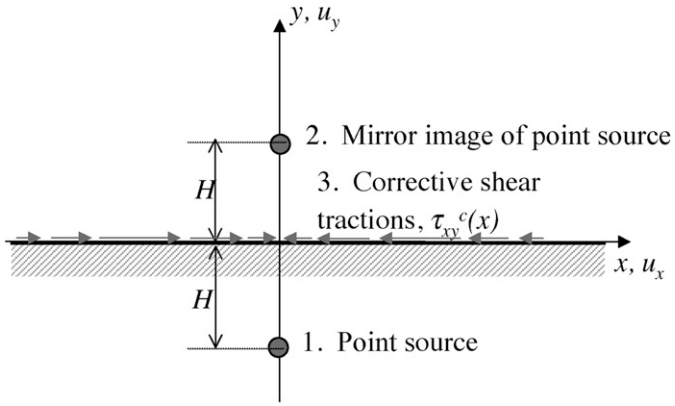

Fig. 5. Superposition of singularity solutions for shallow tunnel (adapted from Sagaseta 1987)

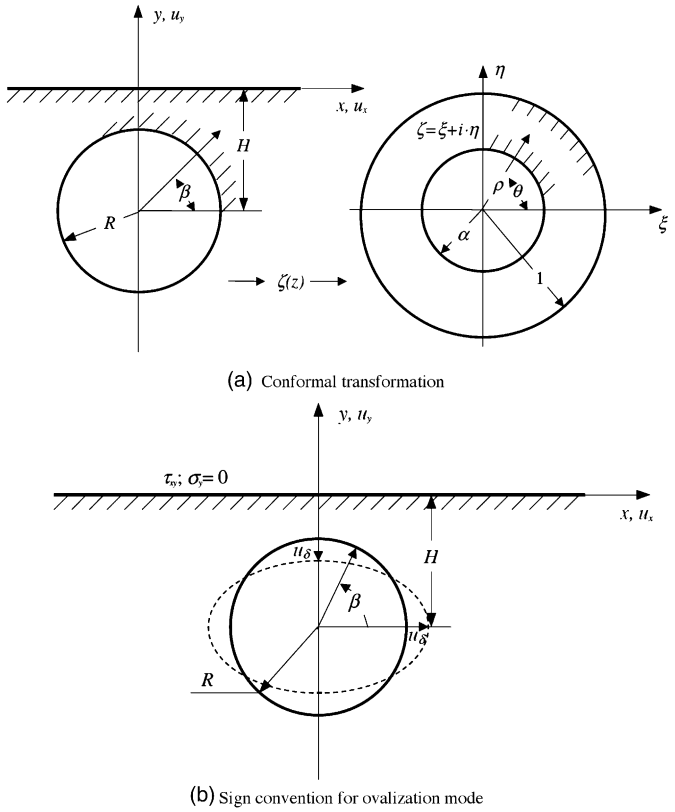

Fig. 6. Conformal transformation for shallow tunnel: (a) conformal transformation; (b) sign convention for ovalization mode (adapted from Verruijt 1996)

circular tunnel cavity boundary transforms to a circle of radius α (note $\alpha < 1$).

As the Goursat functions are analytic, they can be expanded in Laurent series in the transformed domain as follows:

$$\phi(\zeta) = a_0 + \sum_{k=1}^{\infty} a_k \zeta^k + \sum_{k=1}^{\infty} b_k \zeta^{-k}$$
$$\psi(\zeta) = c_0 + \sum_{k=1}^{\infty} c_k \zeta^k + \sum_{k=1}^{\infty} d_k \zeta^{-k} \tag{10}$$

where the coefficients a_k, b_k, c_k, and d_k are found by means of recursive relations derived from the boundary conditions. The stress-free boundary condition at the ground surface [see Verruijt (1997) for full details] yields the following recursive relations for the c_k and d_k coefficients:

$$c_0 = -\overline{a}_0 - \frac{1}{2}a_1 - \frac{1}{2}b_1 \tag{11a}$$

$$c_k = -\overline{b}_k + \frac{1}{2}(k-1)a_{k-1} - \frac{1}{2}(k+1)a_{k+1} \tag{11b}$$

$$d_k = -\overline{a}_k + \frac{1}{2}(k-1)b_{k-1} - \frac{1}{2}(k+1)b_{k+1} \tag{11c}$$

The a and b coefficients are found by imposing the displacement boundary condition at the tunnel wall

$$(1-\alpha^2)\overline{a}_1 - (\kappa+\alpha^2)b_1 = A_0 - (\kappa+1)a_0 \tag{12a}$$

$$(1+\kappa\alpha^2)\overline{a}_1 + (1-\alpha^2)b_1 = \overline{A}_1\alpha + (\kappa+1)\alpha^2\overline{a}_0 \tag{12b}$$

$$(1-\alpha^2)(k+1)\overline{a}_{k+1} - (\alpha^2+\kappa\alpha^{-2k})b_{k+1} = (1-\alpha^2)k\overline{a}_k - (1+\kappa\alpha^{-2k})b_k + A_{-k}\alpha^{-k}, \quad k = 1, 2, \ldots \tag{12c}$$

$$(1+\kappa\alpha^{2\cdot k+2})\overline{a}_{k+1} + (1-\alpha^2)(k+1)b_{k+1} = (1-\alpha^2)kb_k + \alpha^2(1+\kappa\alpha^{2k})\overline{a}_k + \overline{A}_{k+1}\alpha^{k+1}, \quad k = 1, 2, \ldots \tag{12d}$$

where the A_k coefficients define the boundary condition in Fourier series terms as follows:

$$A_k = \frac{1}{2\pi}\int_0^{2\pi} 2G(1-\alpha e^{i\theta})u_z(e^{i\theta})e^{-ik\theta}d\theta \tag{13}$$

Thus, the solution is obtained by solving the integral in Eq. (13) for the Fourier coefficients and then obtaining the Laurent series coefficients by means of Eqs. (11) and (12). Only the value of a_0 remains undetermined. It is obtained from the condition that the coefficients of the expansions must vanish for large k (a requirement for convergence). This is done by means of taking advantage of the linearity of the recursive relations. Hence, two tentative values of a_0 are used to calculate an approximate value of a_∞ and the value that makes $a_\infty = 0$ is found by linear interpolation. Further details are given in the work of Verruijt (1997).

Verruijt (1997) studies the uniform convergence of the tunnel wall, where it is shown that only two Fourier coefficients are needed for this deformation mode (see Appendix II).

The boundary for the case of ovalization of the tunnel cavity can be written in the original plane (Fig. 1) as

$$u_z(\beta) = u_\delta e^{-i\beta} = u_\delta \frac{R}{z(\beta)+iH} \tag{14a}$$

and this becomes transformed according to Eq. (9*a*) into

$$u_z(e^{i\theta}) = u_\delta i\frac{1-\alpha e^{i\theta}}{e^{i\theta}-\alpha} \tag{14b}$$

where $\alpha e^{i\theta}$ represents the mapped coordinate ζ at the tunnel boundary. Thus, the Fourier coefficients for the ovalization mode are found by replacing Eq. (16*b*) into Eq. (13) and performing the integral analytically

$$A_k = \frac{1}{2\pi}\int_0^{2\pi} 2G\frac{\left(1-\alpha e^{i\theta}\right)^2}{e^{i\theta}-\alpha}u_\delta i e^{-ki\theta}d\theta \tag{15}$$

Appendix II summarizes the values of the coefficients, A_k, for the ovalization mode of the tunnel cavity. Only a few terms are needed to achieve an accurate mapping of the boundary deformations (for practical values with $R/H < 0.7$). The full solution for the ovalization mode is thus obtained by means of the recursive relations [Eqs. (11) and (12)].

Evaluations of the Goursat functions [Eq. (8*a*); Pinto 1999] show that 10–15 terms are sufficient to achieve accurate solutions for both the convergence and ovalization modes of deformation.

Results and Comparison of Solutions

One key aspect of the preceding exact formulation is that the half plane is unrestrained and hence, rigid body motions remain undefined. This shortcoming is addressed by Verruijt (1996) by assuming that displacements vanish at infinity. This generates a vertical translation of the tunnel cavity, Δu_y, which produces parasitic differences in the displacements predicted at the crown and inverts of the tunnel cavity for both the convergence and ovalization modes. Figs. 7(a and b) compare the vertical rigid body translation from the exact analyses with approximate solutions at the tunnel axis [Eq. (7)]. The results are in remarkably close agreement for tunnels with radius-embedment ratios, $R/H < 0.5$, over the full range of expected elastic Poisson's ratios. However, approximations in the singularity superposition method become more apparent for very shallow tunnels ($R/H > 0.5$), especially in the ovalization mode.

Fig. 8 compares the spatial distribution of ground movements for a tunnel with $R/H = 0.45$ and $\nu = 0.25$ using the exact and approximate methods of analysis for uniform convergence and ovalization modes of cavity deformation. It should be noted that the vertical displacements (u_y/u_ε and u_y/u_δ) are always symmetric about the y-axis while the horizontal components (u_x/u_ε and u_x/u_δ) are antisymmetric. Although the results are generally in very good agreement, it can be noted that the approximate analysis generates higher vertical displacements that are 10 (u_y/u_ε) and 20% (u_y/u_δ) higher than the exact solutions above the tunnel crown and up to 10% higher for the ovalization-induced horizontal movements (u_x/u_δ). These represent practical upper limits on the differences in the two sets of analyses for this case involving a very shallow tunnel; and further, provide strong justification for using the approximate elastic solutions for subsequent evaluations of tunnel-induced ground movements.

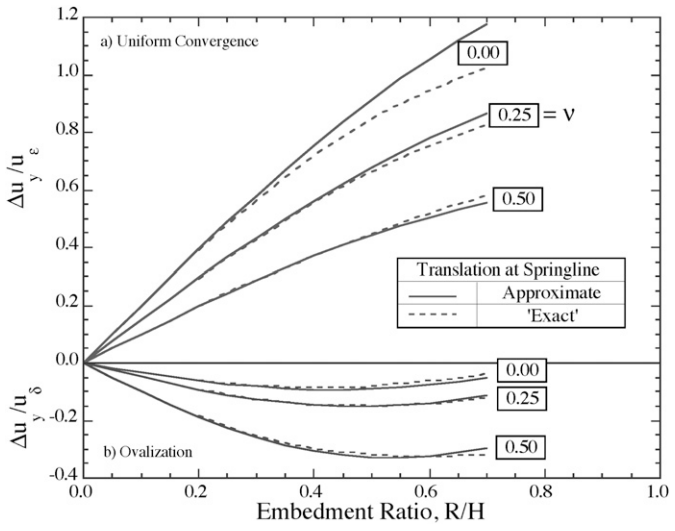

Fig. 7. Comparison of approximate and exact solutions for translation of a shallow tunnel

A uniform contraction (i.e., $u_\varepsilon < 0$) along the tunnel wall, together with the corresponding vertical translation [Eq. (7)], Fig. 7(a), leads to downward displacements everywhere within the soil mass, except in an approximately circular region centered at $y = y_c$ with radius R_c

$$\frac{y_c}{H} = -\frac{2(1-\nu)+1+\sqrt{1+4(1-\nu)^2}}{4(1-\nu)} \tag{16a}$$

$$\frac{R_c}{H} = \frac{\sqrt{1+4(1-\nu)^2}-(1-2\nu)}{2(1-\nu)} \tag{16b}$$

This zone of heave generally lies below the soffit of the tunnel [e.g., Fig. 8(b)]. All points in the soil mass displace horizontally toward the centerline when there is a uniform contraction of the cavity. These general patterns of ground movement are independent of the parameters R/H and ν.

The components of ground surface displacements for the uniform convergence mode can be derived analytically from the approximate method of analysis

$$\frac{u_y}{u_\varepsilon} = 4(1-\nu)\frac{R}{H}\frac{1}{\left(\frac{x}{H}\right)^2+1} \tag{17a}$$

$$\frac{u_x}{u_\varepsilon} = 4(1-\nu)\frac{R}{H}\frac{x}{H}\frac{1}{\left(\frac{x}{H}\right)^2+1} \tag{17b}$$

Fig. 9(a) shows that these solutions represent a good approximation of the exact solutions for practical ranges of the tunnel embedment ($R/H < 0.5$) and elastic Poisson's ratio. The maximum components of the surface displacement are given by

$$\begin{aligned} \frac{u_x|_{\max}}{u_\varepsilon} &= \pm 2\frac{R}{H}(1-\nu) \quad \text{at } x/H = \pm 1 \\ \frac{u_y^0}{u_\varepsilon} &= \frac{u_y|_{\max}}{u_\varepsilon} = 4\frac{R}{H}(1-\nu) \quad \text{at } x/H = 0 \end{aligned} \tag{18}$$

Hence, $u_y|_{\max} = 2u_x|_{\max}$, and $u_y = u_x$ at $x = H$.

The area (ΔV_s) enclosed by the deformed settlement trough can be evaluated from Eq. (17), using the conventional assumption that only vertical displacements contribute to this volume, given by

$$\Delta V_s = 4\pi u_\varepsilon R(1-\nu) \equiv 2(1-\nu)\Delta V_L \equiv \pi H u_y^0 \tag{19}$$

This result shows that the volume loss at the ground surface is equal to the volume loss at the tunnel cavity (i.e., $\Delta V_s = \Delta V_L$) for $\nu = 0.5$, while $\Delta V_s = 2\Delta V_L$ for $\nu = 0$ (as noted by Verruijt and Booker 1996).

Typical results for the ovalization mode, Figs. 8(c and d), show that a positive distortion of the tunnel cavity ($u_\delta > 0$) produces a zone of settlement above the tunnel spring line and extending laterally to $|x/H| \le 1$, with heave occurring in the far field and below the spring line. The soil undergoes outward horizontal movements except in

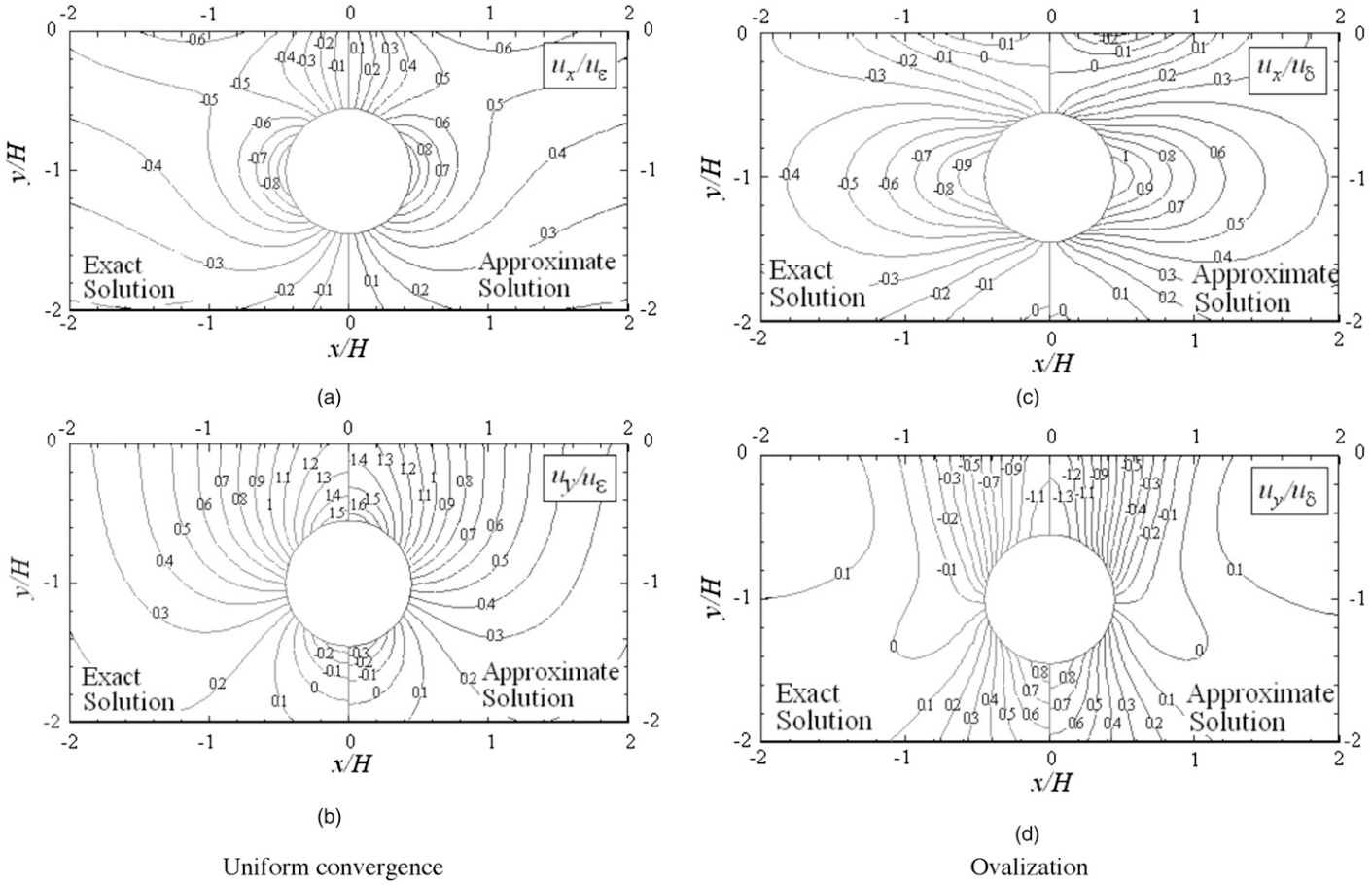

Fig. 8. Comparison of ground deformations for shallow tunnel, $R/H = 0.45$, in elastic soil with $\nu = 0.25$ using approximate and exact methods of analysis

a triangular zone where it extends from the crown to the ground surface (at $|x/H| \leq 1$) and below the soffit. There is only a small dependence in this pattern of behavior with R/H and ν.

The magnitudes of the surface displacement components from the approximate analyses of the ovalization mode are as follows:

$$\frac{u_y}{u_\delta} = 2\frac{R}{H}\frac{4(1-\nu)}{3-4\nu}\frac{\left[\left(\frac{x}{H}\right)^4 - 1\right] + \frac{1}{4(1-\nu)}\left(\frac{R}{H}\right)^2\left[1 - 3\left(\frac{x}{H}\right)^2\right]}{\left[\left(\frac{x}{H}\right)^2 + 1\right]^3} \tag{20a}$$

$$\frac{u_x}{u_\delta} = 2\frac{R}{H}\frac{4(1-\nu)}{3-4\nu}\frac{x}{H}\frac{\left(\frac{x}{H}\right)^2 - 1}{\left[\left(\frac{x}{H}\right)^2 + 1\right]^2} \tag{20b}$$

These results can be further simplified using the far field approximation [cf. Eqs. (3*a*)–(3*c*)]

$$\frac{u_x(x)}{u_\delta} = 2\frac{R}{H}\frac{4(1-\nu)}{3-4\nu}\frac{x}{H}\frac{\left(\frac{x}{H}\right)^2 - 1}{\left[\left(\frac{x}{H}\right)^2 + 1\right]^2} \tag{20c}$$

$$\frac{u_y(x)}{u_\delta} = 2\frac{R}{H}\frac{4(1-\nu)}{3-4\nu}\frac{\left(\frac{x}{H}\right)^2 - 1}{\left[\left(\frac{x}{H}\right)^2 + 1\right]^2} \tag{20d}$$

Ovalization produces a minimum surface settlement at the centerline (i.e., a maximum surface settlement) and a far field maximum heave

$$\frac{u_y|_{\min}}{u_\delta} = -2\frac{R}{H}\frac{4(1-\nu)}{3-4\nu}\left[1 - \frac{1}{4(1-\nu)}\left(\frac{R}{H}\right)^2\right] \quad \text{at } x = 0$$
$$\frac{u_y|_{\max}}{u_\delta} \approx \frac{R}{H}\frac{1-\nu}{3-4\nu} \quad \text{at } \frac{x}{H} = \pm\sqrt{3} \tag{21a}$$

There are also two maxima in the horizontal surface displacements

$$\frac{u_x}{u_\delta} = \pm\frac{R}{H}\frac{2(1-\nu)}{3-4\nu} \quad \text{at } \frac{x}{H} = \pm 1 \mp \sqrt{2} \tag{21b}$$

therefore, the maximum inward movement occurs at $x/H = \pm 0.4142$ and there is an equal, outward displacement at $x/H = \pm 2.4142$.

The preceding discussion has summarized the characteristic ground movements resulting from uniform convergence and

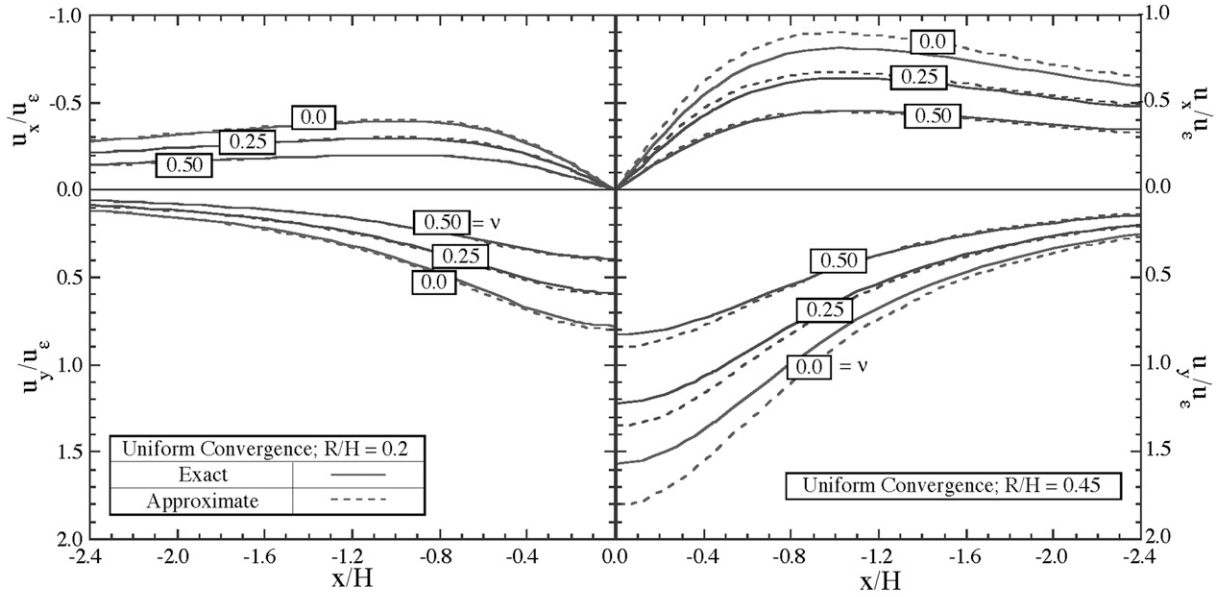

(a) Surface displacements for uniform convergence mode

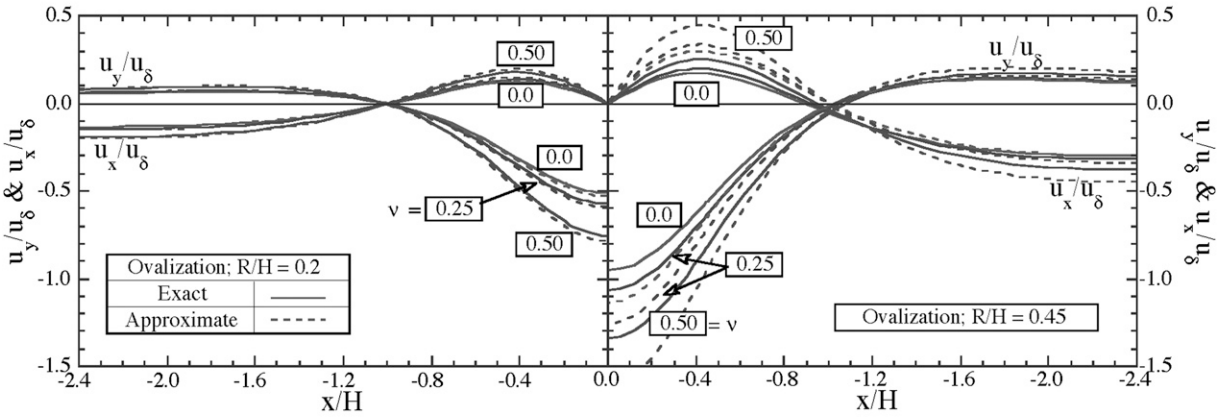

(b) Surface displacements for ovalization mode

Fig. 9. Comparison of exact and approximate analyses for surface displacements for (a) uniform convergence mode; (b) ovalization mode

ovalization deformations, u_ε and u_δ at the tunnel cavity in an isotropic, elastic soil. Approximate analyses derived by superposition of singularity solutions provide a very good approximation of the more complete analyses using complex variables for all cases except very shallow tunnels ($R/H > 0.5$).

Fig. 10 shows the combined effects of the convergence and ovalization modes on the predicted surface settlements

$$\frac{u_y}{u_\varepsilon} = 4(1-\nu)\frac{R}{H}\frac{\dfrac{-2\rho}{3-4\nu}\left\{\left[\left(\dfrac{x}{H}\right)^4 - 1\right] - \dfrac{1}{4(1-\nu)}\left[3\left(\dfrac{x}{H}\right)^2 - 1\right]\left(\dfrac{R}{H}\right)^2\right\} + \left[\left(\dfrac{x}{H}\right)^2 + 1\right]^2}{\left[\left(\dfrac{x}{H}\right)^2 + 1\right]^3} \tag{22}$$

where $\rho = -u_\delta/u_\varepsilon$ = relative distortion of the tunnel cavity.

There is negligible variation of the resulting settlement distribution with the embedment ratio, R/H, and only a small narrowing of the settlement trough as Poisson's ratio increases from $\nu = 0.0$ to 0.5. The main parameter affecting the distribution of surface settlement is the relative distortion of the tunnel cavity, ρ. As ρ is increased from 0.0 (uniform convergence) to 3.0, there is a marked narrowing of the settlement trough. For high values of ρ

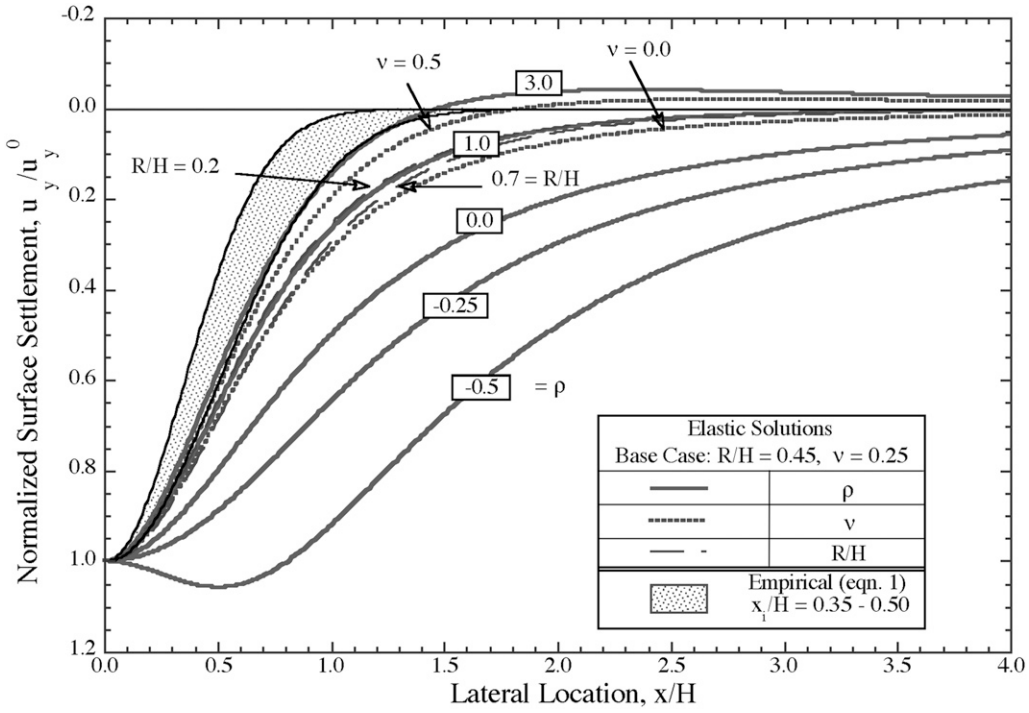

Fig. 10. Comparison of surface settlement trough shapes for shallow tunnels in isotropic elastic soil

it is possible to achieve a first-order agreement with empirical measurements. In contrast, when $\rho < 0$, the analyses predict that maximum settlement does not occur above the centerline of the tunnel.

Effects of Yielding of Ground Mass

One of the key limitations of the analytical solutions is the assumption that soil behavior can be approximated by linear elasticity. The effects of soil plasticity can be understood by considering the case of uniform convergence around a deep tunnel [equivalent to conditions with $K_0 = 1.0$; Eq. (2)]. Most recently, Schürch and Anagnostou (2012) have also reported for tunnels in Mohr-Coulomb soils with nonisotropic stress states (focusing mainly on the ground response curves). Classical plasticity solutions (e.g., Brown et al. 1983; Yu and Rowe 1999) obtain closed-form solutions for the soil stresses and displacements due to cavity contraction in a linearly–elastic, plastic material with Mohr-Coulomb yielding (c', ϕ') and nonassociative flow at constant dilation angle, ψ

$$\frac{\varepsilon^p_{\text{vol}}}{\gamma^p} = -\sin\psi \tag{23}$$

where $\varepsilon^p_{\text{vol}}$ = plastic volumetric strain; and γ^p = maximum plastic shear strain.

For the case of undrained shear in low permeability clays ($c' \to s_u$, $\phi' = 0° = \psi$), the incompressibility constraint controls the displacement field and there are no effects of plasticity on the deformation field (i.e., the displacement field coincides with the linear elastic solutions reported in the preceding sections for a given cavity convergence.

In the more general case, dilative volumetric strains can produce significant changes in the deformation within the plastic zone around the tunnel cavity. In this case, the elastic solution will typically underestimate the strains occurring at the tunnel cavity. The strain necessary to cause yielding at the cavity is given by

$$\frac{u^y_\varepsilon}{R} = -\frac{(N_\phi - 1) + \overline{Y}}{2\overline{G}(N_\phi + 1)} \tag{24}$$

where $\overline{Y} = (2c'/p'_0)[\cos\phi'/(1-\sin\phi')]$; $N_\phi = (1+\sin\phi')/(1-\sin\phi')$; $\overline{G} = G/p'_0$; G = linear shear modulus; and p'_0 = initial mean effective stress. The radius of plastic yielding, R_p, can then be obtained as

$$\frac{R_p}{R} = \left(\frac{u^p_\varepsilon}{u^y_\varepsilon}\right)^{1/(1+\beta)} \tag{25}$$

where u^p_ε = radial displacement at the tunnel cavity (neglecting elastic strains within the plastic zone as noted by Kovári 1985); and $\beta = (1+\sin\psi)/(1-\sin\psi)$

Fig. 11(a) illustrates the dimensions of the plastic zone for typical ranges of soil properties. The two principal parameters affecting the size of the plastic zone are the preyield stiffness ($\overline{G}$) and the dilation angle, ψ [Fig. 11 assumes $\psi = (\phi' - \phi_{cv})$, where the constant volume friction angle, $\phi_{cv} = 30°$]. The plastic zone increases in size with the soil stiffness and reduces with increased dilation angle.

For situations where the plastic zone does not extend to the ground surface, there is a simple link between the actual convergence strain at the tunnel cavity and the equivalent elastic solution that can be defined through a reduction factor, RF [Fig. 11(b)]

$$\text{RF} = \frac{u^e_\varepsilon}{u^p_\varepsilon} = \left(\frac{u^p_\varepsilon}{u^y_\varepsilon}\right)^{(1-\beta)/(1+\beta)} \tag{26}$$

For situations where plasticity extends to the ground surface, there are no analytical solutions available for estimating the ground movements. However, an intriguing approximation has been proposed by González and Sagaseta (2001) based on the observation that displacements within the plastic zone are functions of $1/r^\beta$ (neglecting elastic strain components). Hence, the displacements around a deep tunnel [cf. Eq. (3*a*)] in a dilating plastic soil can be written

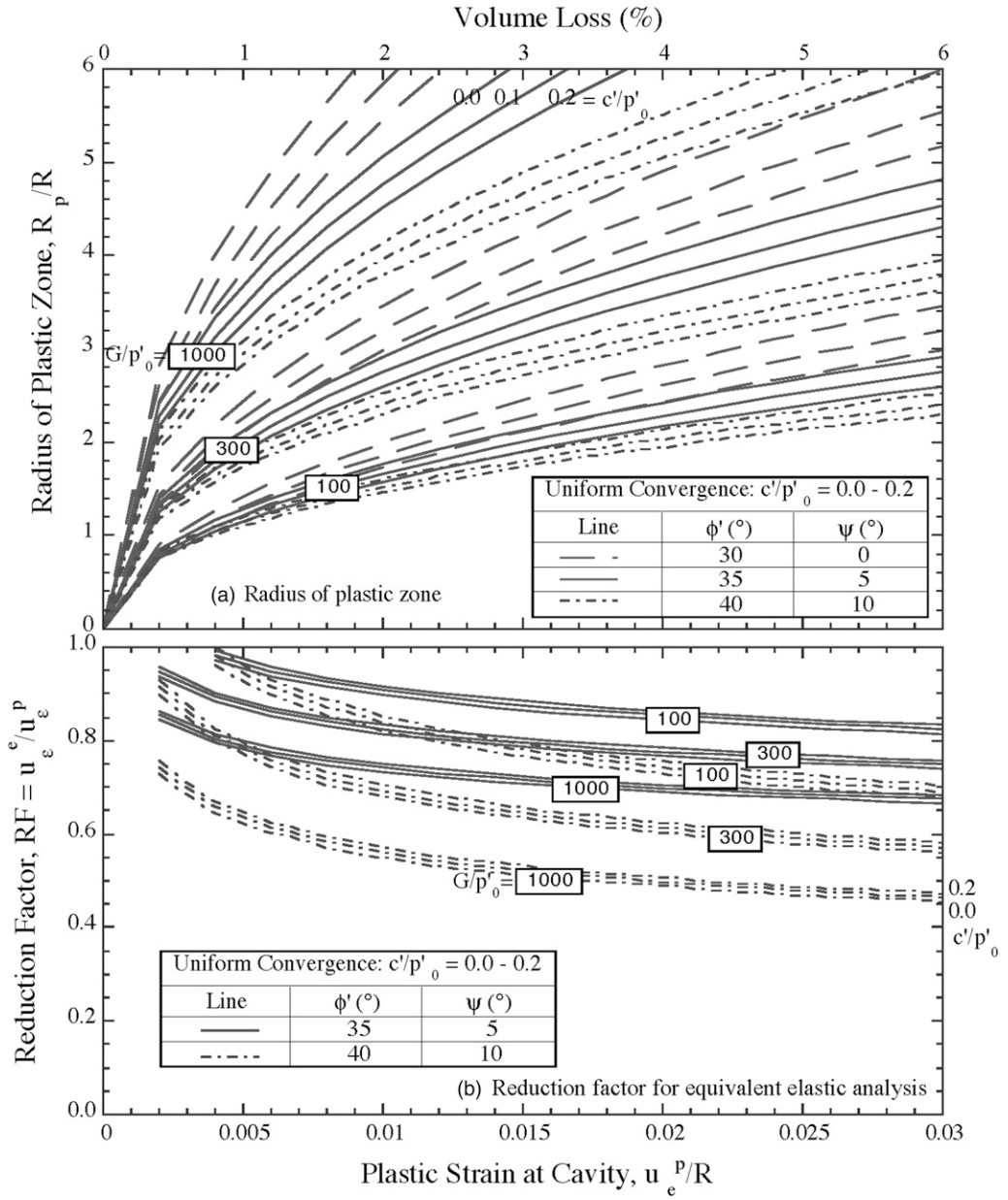

Fig. 11. Radial dimension of plastic zone for uniform convergence of deep tunnel in elastoplastic soil: (a) radius of plastic zone; (b) reduction factor for equivalent elastic analysis

$$\text{Convergence:} \begin{cases} u_x(x,y) = u_\varepsilon \dfrac{xR^{\alpha-1}}{\left(x^2+y^2\right)^\alpha} \\ u_y(x,y) = u_\varepsilon \dfrac{yR^{\alpha-1}}{\left(x^2+y^2\right)^\alpha} \end{cases} \tag{27}$$

where $\alpha = (\beta+1)/2$. It should be noted again that there is coincidence of the displacement fields for the linearly elastic and perfectly plastic cases ($\psi = 0°$, $\beta = 0$).

Following this logic, solutions for a shallow tunnel can be found by the approximate singularity superposition method as shown in Appendix III. The results retain many of the same features of the elastic solution and the distribution of ground deformations is now controlled by two parameters, $\rho\,(=-u_\varepsilon,/u_\delta)$ and α. Assuming a maximum dilation rate, $\psi = 30°$, the parameter α ranges from 1.0–2.0. Fig. 12 illustrates the effects of the dilation angle on computed surface settlements for a tunnel with embedment ratio, $R/H = 0.45$. The results show that increasing the dilation causes a significant narrowing of the surface settlement trough for the uniform convergence case ($\rho = 0$). Further narrowing occurs when ovalization is included. The results in Fig. 12 show good agreement between empirical estimates of the trough shape [Eq. (1)] and the analytic solutions for $\rho = 1.0$.

Three-Dimensional Effects

The previous sections have shown that simplified analytical solutions based on singularity superposition can provide a good approximation for 2D ground deformations around shallow tunnels and can achieve reasonable agreement with empirically observed settlement troughs by accounting for different modes of deformation at the tunnel cavity (relative distortion) or dilative volumetric strains (in free or partially draining soils). It is also possible to account for anisotropy in soil

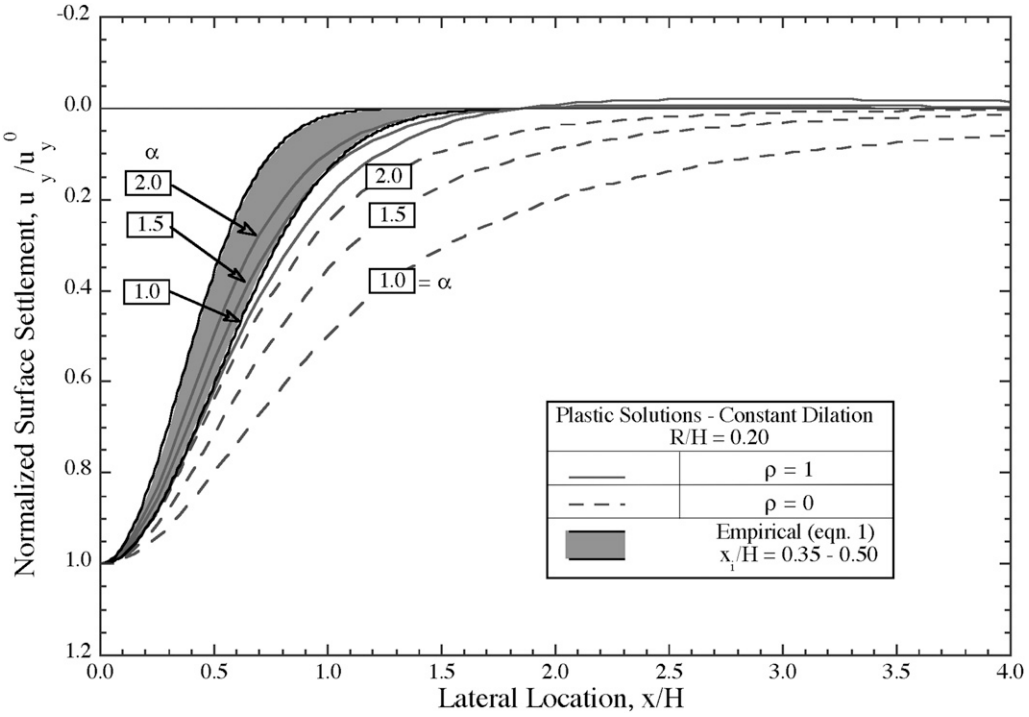

Fig. 12. Effects of soil dilation on surface settlement trough shape

stiffness (Zymnis et al. 2013) and this section illustrates the extension for modeling 3D deformation fields around a tunnel heading.

Appendix IV summarizes the derivation of 3D ground movements for a spherical cavity point contraction embedded at depth, H, in an elastic half-space based on the method of singularity superposition (after Sagaseta 1987; Sen 1950; Mindlin and Cheng 1950). The displacement components can be expressed as follows:

$$u_x = \frac{V_L}{4\pi} f(x,y,z), \quad u_y = \frac{V_L}{4\pi} g(x,y,z), \quad u_z = \frac{V_L}{4\pi} h(x,y,z) \tag{28a}$$

where z = horizontal coordinate parallel to the tunnel axis; and volume loss, V_L, is linked to the radial convergence, u_ε

$$V_L = \frac{u_\varepsilon}{4\pi R^2} \tag{28b}$$

and the functions f, g, and h are shown in Appendix V.

For a cavity located at an arbitrary position along the tunnel axis, $z = \zeta$ the displacements due to a unit ground loss ($V_L = 1$) are

$$\Gamma_x(x,y,z,\zeta) = \frac{1}{4\pi} f(x,y,z-\zeta) \tag{29a}$$

$$\Gamma_y(x,y,z,\zeta) = \frac{1}{4\pi} g(x,y,z-\zeta) \tag{29b}$$

$$\Gamma_z(x,y,z,\zeta) = \frac{1}{4\pi} h(x,y,z-\zeta) \tag{29c}$$

The 3D ground movements around a tunnel heading are then obtained by assuming a volume loss distribution along the tunnel axis, $\Omega(\zeta)\cdot d\zeta$, and integrating along these Green functions along the line

$$u_x = \int_{-\infty}^{0} \Gamma_x(x,y,z,\zeta)\Omega(\zeta)d\zeta \tag{30a}$$

$$u_y = \int_{-\infty}^{0} \Gamma_y(x,y,z,\zeta)\Omega(\zeta)d\zeta \tag{30b}$$

$$u_z = \int_{-\infty}^{0} \Gamma_z(x,y,z,\zeta)\Omega(\zeta)d\zeta \tag{30c}$$

These equations can be integrated numerically for prescribed axial distributions of ground loss (e.g., to account for different methods of tunnel excavation and support). This paper considers the simplest case where the volume loss is uniformly distributed with $\Omega(\zeta) = V_{2D} = 2\pi R u_\varepsilon$, along the length of the tunnel from $-\infty \le z \le 0$. In this case, the displacement field can be solved analytically as follows:

$$u_x = \frac{V_{2D}}{4\pi}\left\{\frac{x(R_1-z)}{r_1^2 R_1} + \frac{(3-4\nu)x(R_2-z)}{r_2^2 R_2} + \frac{xy(y-H)\left[2z(3R_2^2-z^2)-4R_2^3\right]}{r_2^4 R_2^3}\right\} \tag{31a}$$

$$u_y = \frac{V_{2D}}{4\pi}\left\{\frac{(y+H)(R_1-z)}{r_1^2 R_1} + \frac{2y(y-H)^2\left[z(3R_2^2-z^2)-2R_2^3\right]}{r_2^4 R_2^3} - \frac{[(3-4\nu)(y-H)-2H](R_2-z)-2(R_2-z)(y-H)}{r_2^2 R_2}\right\} \tag{31b}$$

$$u_z = \frac{V_{2D}}{4\pi}\left\{\frac{1}{R_1} + \frac{(3-4\nu)}{R_2} - \frac{2y(y-H)}{R_2^3}\right\} \tag{31c}$$

where $r_1 = \sqrt{x^2 + (y+H)^2}$, $r_2 = \sqrt{x^2 + (y-H)^2}$, and

$$R_1 = \sqrt{x^2 + z^2 + (y+H)^2}, \quad R_2 = \sqrt{x^2 + z^2 + (y-H)^2}$$

The ground surface displacements can then be found as

$$u_x|_{y=0} = \frac{V_{2D}}{\pi}\frac{(1-\nu)x}{x^2+H^2}\frac{\sqrt{x^2+z^2+H^2}-z}{\sqrt{x^2+z^2+H^2}} \tag{32a}$$

$$u_y|_{y=0} = \frac{V_{2D}}{\pi}\frac{(1-\nu)H}{x^2+H^2}\frac{\sqrt{x^2+z^2+H^2}-z}{\sqrt{x^2+z^2+H^2}} \tag{32b}$$

$$u_z|_{y=0} = \frac{V_{2D}}{\pi}\frac{(1-\nu)}{\sqrt{x^2+z^2+H^2}} \tag{32c}$$

It is interesting to note that the surface settlements, u_y, are related to the transverse horizontal displacement components, $u_x = xu_y/H$. Fig. 13 shows contours of surface displacements for a tunnel with embedment, $R/H = 0.2$, while Figs. 14(a–c) examine the surface settlement distribution. The results show that 3D effects are limited to a zone around the tunnel heading $-2 \le z/H \le 2$. For example, the longitudinal distribution, Fig. 14(b) shows surface settlements occurring up to $2H$ ahead of the advancing tunnel heading and converging to a steady state for $z/H \le -2$. Centerline surface settlements at the tunnel heading ($z/H = 0$), Fig. 14(b) correspond to approximately 50% of those occurring far behind the heading ($z/H < -2$). There is little variation in the normalized transverse settlement trough (u_z/u_z^0) [Fig. 14(c)] for $z/H \le 0$. These general features of behavior are related to the assumption of a uniform ground loss along the tunnel axis and can clearly be refined to represent different methods of tunnel construction.

Conclusions

The analytical solutions presented in this paper describe the far field ground movements caused by shallow tunneling processes (excavation and support) as functions of deformations occurring at the tunnel cavity in 2D for idealized modes of uniform convergence and ovalization (defined by parameters u_ε and u_δ, respectively). Closed-form solutions obtained by superposition of singularity solutions (after Sagaseta 1987) provide a good approximation of the more complete (exact) solutions obtained by representing the finite radial dimensions of a shallow tunnel in an elastic soil (after Verruijt 1996), while both sets of solutions generate parasitic vertical translation components of the tunnel cavity (Fig. 7). This latter behavior has been a source of confusion in prior applications and (semiempirical) modifications of the analytical solutions (e.g., Loganathan and Poulos 1998). The elastic solutions are able to replicate empirical estimates of the transverse distribution of surface settlements only for relatively large cavity distortions, $\rho\,(= -u_\varepsilon/u_\delta) > 1$.

Plastic yielding has no effect on the incompressible deformation fields associated with (short-term) undrained shearing of low permeability clays. However, dilation of free- or partially-draining soils can have a significant influence on the distribution of tunnel-induced ground movements and may explain the very narrow settlement troughs measured for tunnels in sands. This behavior appears to be well described using approximate analytical solutions for plastic soils with a constant angle of dilation.

The current paper also illustrates the extension of the analyses for 3D ground movements around a shallow tunnel heading. Fundamental solutions have been developed for uniform convergence of a shallow spherical cavity in an elastic soil half-space. Results for the case where ground loss is distributed uniformly along the tunnel axis show that 3D effects are limited to a region within distance, $z/H = \pm 2$ of the tunnel heading. Further research is now needed to obtained analytic solutions for ovalization of a shallow spherical cavity and hence, to generalize the 3D analyses to account for relative distortions along the tunnel axis.

Appendix I. Derivation of Displacements due to Corrective Surface Tractions

The unbalanced shear stresses, τ_{xy}, at the surface are calculated according to the classical expression derived from theory of elasticity

$$\tau_{xy} = G\left[\frac{\partial u_y}{\partial x} + \frac{\partial u_x}{\partial y}\right] \tag{33}$$

where u_x and u_y = displacements due to the singularity solutions [Eqs. (3a) and (3b)].

The Airy stress function, $F(x,y)$, can then be determined from an inverse Fourier transform

$$F(x,y) = \frac{i}{2\pi}\int_{-\infty}^{\infty} \mathrm{T}_{xy}(\omega)\frac{y}{\omega}e^{|\omega|y}e^{i\omega x}d\omega \tag{34}$$

where $T_{xy}(\omega)$ is the Fourier transform of the correction surface tractions along the ground surface (plane with $y = 0$)

$$\mathrm{T}_{xy} = \int_{-\infty}^{\infty} \tau(x)e^{-i\omega x}dx \tag{35}$$

The corrective displacements [Eqs. (6a) and (6b)] are then obtained from the Airy stress function displacements following standard methods of elasticity (e.g., Boresi and Chong 1987)

$$\begin{aligned} u_x &= \frac{1}{2G}\left[(1-\nu)q_1 - \frac{\partial F}{\partial x}\right] \\ u_y &= \frac{1}{2G}\left[(1-\nu)q_2 - \frac{\partial F}{\partial y}\right] \end{aligned} \tag{36}$$

where

$$q_1 + iq_2 = \int (Q_1 + iQ_2)dz \tag{37a}$$

$$Q_1 = \nabla^2 F \tag{37b}$$

and Q_2 is the harmonic conjugate of Q_1

$$\frac{\partial Q_1}{\partial x} = \frac{\partial Q_2}{\partial y}; \quad \frac{\partial Q_1}{\partial y} = -\frac{\partial Q_2}{\partial x} \tag{37c}$$

Appendix VI summarizes the specific results of Eqs. (33)–(37) for the uniform convergence and ovalization singularity solutions.

J. Geotech. Geoenviron. Eng. 2014.140.

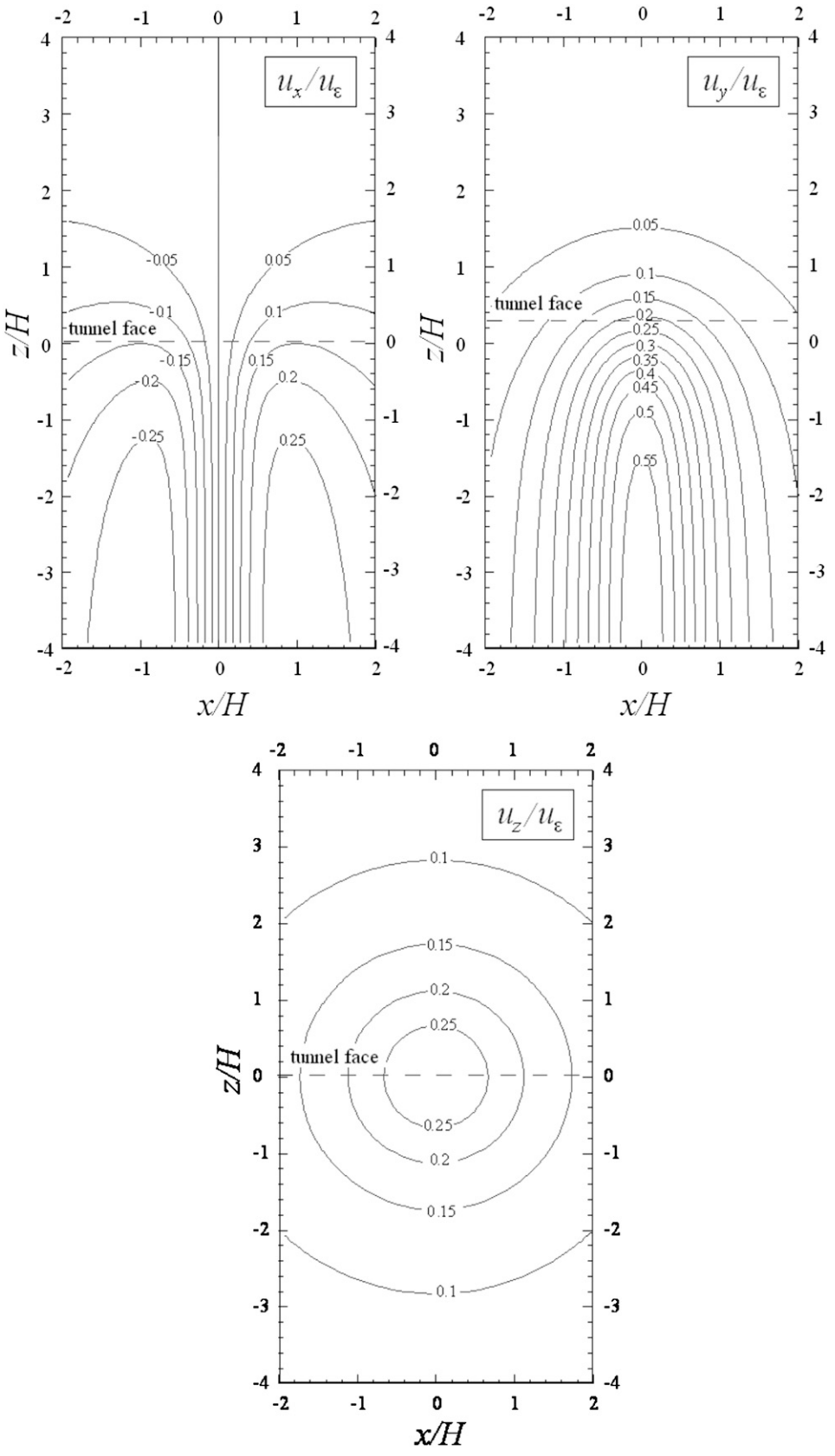

Fig. 13. Contours of 3D surface displacement components for shallow tunnel in elastic soil with uniform ground loss and $R/H = 0.2$, $\nu = 0.25$

Appendix II. Fourier Coefficients for Boundary Deformations of Tunnel Cavity

Uniform Convergence

$$A_k = 0 \quad \forall k < 0$$

$$A_0 = 2iGu_\varepsilon\alpha$$

$$A_1 = -2iGu_\varepsilon$$

$$A_k = 0 \quad \forall k > 1$$

Ovalization

$$A_k = 2Gu_\delta i\left[\alpha^{-(k+1)}\left(1-\alpha^2\right)^2\right] \quad \forall k < 0$$

$$A_0 = 2Gu_\delta i\alpha\left(\alpha^2 - 2\right)$$

$$A_1 = 2Gu_\delta i\alpha^2$$

$$A_k = 0 \quad \forall k > 1$$

Appendix III. Displacement Components for Tunnel in Plastic, Dilating Soil

Uniform Convergence Mode

$$\frac{u_x}{u_\varepsilon R^{2\alpha-1}} \quad \left\{ \frac{x}{\left[x^2+(y+H)^2\right]^\alpha} - \frac{x}{\left[x^2+(y-H)^2\right]^\alpha} + \frac{2x}{\left[x^2+(y-H)^2\right]^\alpha} - 4\frac{(y-H)xy}{\left[x^2+(y-H)^2\right]^{\alpha+1}} \right.$$

$$\frac{u_y}{u_\varepsilon R^{2\alpha-1}} \quad \left\{ \frac{(y+H)}{\left[x^2+(y+H)^2\right]^\alpha} - \frac{(y-H)}{\left[x^2+(y-H)^2\right]^\alpha} + \frac{4(y-H)x^2 + 2H\left[x^2-(y-H)^2\right]}{\left[x^2+(y-H)^2\right]^{\alpha+1}} - \frac{2(y-H)}{\left[x^2+(y-H)^2\right]^\alpha} \right.$$

Ovalization Mode

$$\frac{u_x}{u_\delta R^{2\alpha-1}} \quad x \times \left\{ \frac{\left[x^2+(y+H)^2\right]^2 - \left[3(y+H)^2 - x^2\right]\left[x^2+(y+H)^2 - R^2\right]}{\left[x^2+(y+H)^2\right]^{\alpha+2}} \right.$$

$$- \frac{\left[x^2+(y-H)^2\right]^2 - \left[3(y-H)^2 - x^2\right]\left[x^2+(y-H)^2 - R^2\right]}{\left[x^2+(y-H)^2\right]^{\alpha+2}}$$

$$\left. + 4\frac{x^2+y^2-H^2}{\left[x^2+(y-H)^2\right]^{\alpha+1}} - 8y\frac{y\left(x^2+y^2\right) + 2H\left(H^2-x^2\right) - 3yH^2}{\left[x^2+(y-H)^2\right]^{\alpha+2}} \right\}$$

$$\frac{u_y}{-u_\delta R^{2\alpha-1}} \quad \left\{ (y+H)\frac{\left[x^2+(y+H)^2\right]^2 - \left[3x^2 - (y+H)^2\right]\left[x^2+(y+H)^2 - R^2\right]}{\left[x^2+(y+H)^2\right]^{\alpha+2}} \right.$$

$$- (y-H)\frac{\left[x^2+(y-H)^2\right]^2 - \left[3x^2 - (y-H)^2\right]\left[x^2+(y-H)^2 - R^2\right]}{\left[x^2+(y-H)^2\right]^{\alpha+2}}$$

$$\left. - 4\frac{x^2(2H-y) - y(y-H)^2}{\left[x^2+(y-H)^2\right]^{\alpha+1}} + 8\frac{(y-H)\left\{Hy(y-H)^2 - x^2\left[\left(x^2+y^2\right) + H(y+H)\right]\right\}}{\left[x^2+(y-H)^2\right]^{\alpha+2}} \right.$$

J. Geotech. Geoenviron. Eng. 2014.140.

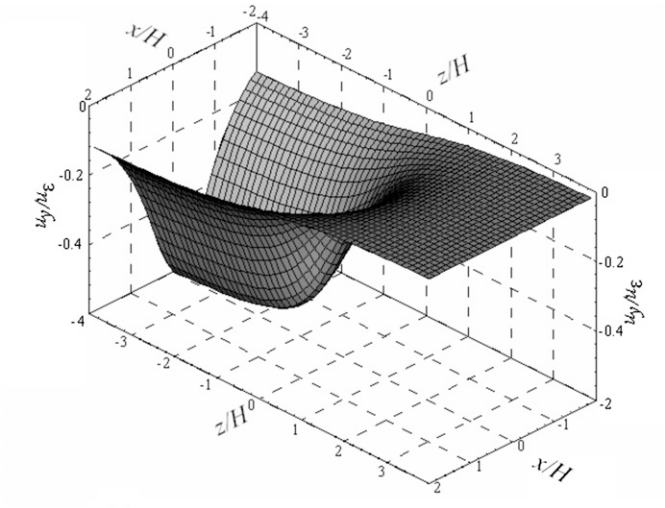

(a) Settlement trough for tunnel with R/H = 0.2, ν = 0.25

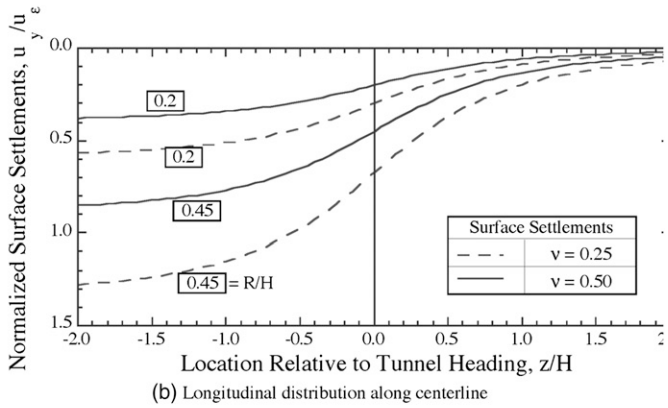

(b) Longitudinal distribution along centerline

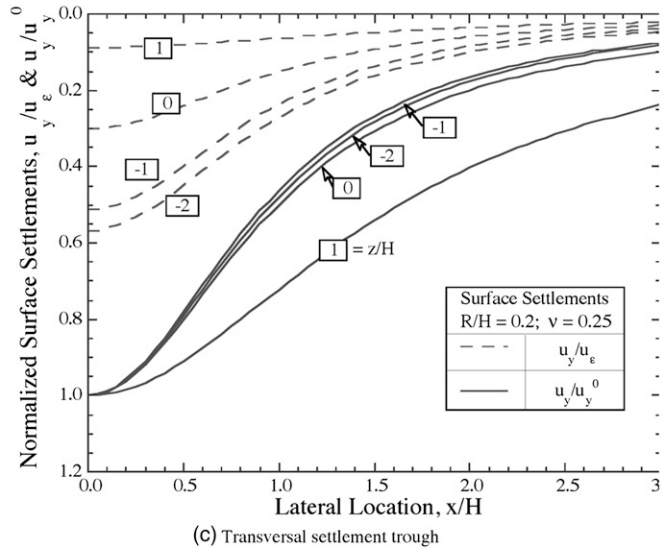

(c) Transversal settlement trough

Fig. 14. 3D surface settlements for shallow tunnel in elastic soil with uniform ground loss: (a) settlement trough for tunnel with $R/H = 0.2$, $\nu = 0.25$; (b) longitudinal distribution along centerline; (c) transversal settlement trough

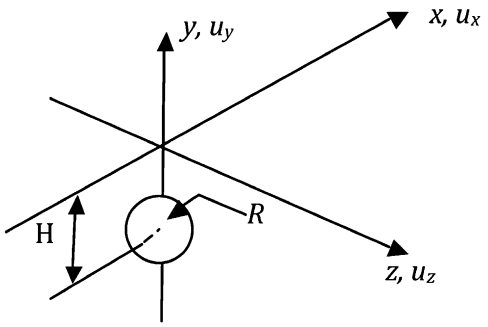

Fig. 15. Spherical cavity contraction

Appendix IV. Three-Dimensional Deformations due to a Shallow Spherical Cavity Contraction

The displacements field due to a cavity contraction (or expansion) in an infinite elastic space is a radial displacement field given by

$$u_r = u_\varepsilon \left(\frac{R}{r}\right)^2 \tag{38}$$

where u_ε is related to the cavity volume as $u_\varepsilon = V_L/4\pi R^2$. To account for a traction-free surface, additional displacements due to the corrective stresses applied in the plane defined by $y = 0$ (see Fig. 15) need to be superimposed. This problem is a classical problem of theory of elasticity and its solution can also be found in Sen (1950) and Mindlin and Cheng (1950).

The solution is obtained by first defining the displacement field in Eq. (38) as the gradient of a potential as follows:

$$\Psi^c = \int u_r dr = -u_\varepsilon \frac{R^2}{r} = -u_\varepsilon \frac{R^2}{\sqrt{x^2 + z^2 + (y+H)^2}} \tag{39}$$

Hence, displacements in different directions are obtained as the gradient of the potential in the direction of interest

$$u_x = u_r \frac{x}{r} = \frac{\partial \Psi}{\partial r}\frac{dr}{dx} = \frac{\partial \Psi}{\partial x} \tag{40}$$

Corrective tractions are then evaluated by means of standard linear elastic constitutive equations such that they oppose the surficial tractions due to the cavity displacement field (see Appendix VII). Following standard solution methods for theory of elasticity, the stress field due to the corrective tractions is obtained in terms of a corrective stress potential

$$\Psi^c = -u_\varepsilon \frac{R^2}{\sqrt{x^2 + z^2 + (y-H)^2}} \tag{41}$$

It is interesting to note that the corrective stress potential represents a mirror image (with respect to the traction-free surface) of the potential due to the cavity. The stress field due to the corrective tractions is given in Appendix VII. The corresponding displacements are thus calculated by integrating linear-elastic constitutive equations and the solution for the cavity contraction in elastic half space is found by adding both displacement fields. The full solution for displacements is given in Appendix V.

Appendix V. Three-Dimensional Displacement Fields for a Spherical Source at Depth H in an Elastic Half-Space

$$f(x,y,z) \quad \frac{x}{\left[x^2+z^2+(y+H)^2\right]^{3/2}} - 6\frac{(y-H)yx}{\left[x^2+z^2+(y-H)^2\right]^{5/2}} + \frac{(3-4\nu)x}{\left[x^2+z^2+(y-H)^2\right]^{3/2}}$$

$$h(x,y,z) \quad \frac{z}{\left[x^2+z^2+(y+H)^2\right]^{3/2}} - 6\frac{(y-H)zy}{\left[x^2+z^2+(y-H)^2\right]^{5/2}} + \frac{(3-4\nu)z}{\left[x^2+z^2+(y-H)^2\right]^{3/2}}$$

$$g(x,y,z) \quad \left\{ \frac{(y+H)}{\left[x^2+z^2+(y+H)^2\right]^{3/2}} - 2y\frac{3(y-H)^2-\left[x^2+z^2+(y-H)^2\right]}{\left[x^2+z^2+(y-H)^2\right]^{5/2}} - \frac{(3-4\nu)(y-H)}{\left[x^2+z^2+(y-H)^2\right]^{3/2}} \right\}$$

Appendix VI. Summary of Derivation of Corrective Tractions

Convergence

For $\tau_{xy}(x)$

$$-8Gu_\varepsilon RH\frac{x}{(x^2+H^2)^2}$$

For $F(x,y)$

$$4Gu_\varepsilon Ry\frac{H-y}{x^2+(y-H)^2}$$

For $Q_1(x,y)$

$$8Gu_\varepsilon R\frac{(y-H)^2-x^2}{\left[(y-H)^2+x^2\right]^2}$$

For $Q_2(x,y)$

$$16Gu_\varepsilon Rx\frac{(y-H)}{\left[(y-H)^2+x^2\right]^2}$$

For $q_1(x,y)$

$$8Gu_\varepsilon R\frac{x}{x^2+(y-H)^2}$$

For $q_2(x,y)$

$$-8Gu_\varepsilon R\frac{(y-H)}{x^2+(y-H)^2}$$

Ovalization

For $\tau_{xy}(x)$

$$\frac{16u_\delta HRGx}{3-4\nu}\frac{\left(x^2-H^2\right)\left[2\left(x^2+H^2\right)-3R^2\right]}{\left(x^2+H^2\right)^4} \approx -\frac{32u_\delta HRGx}{3-4\nu}\frac{x^2-H^2}{\left(x^2+H^2\right)^3}$$

For $F(x,y)$

$$\frac{8u_\delta RG}{3-4\nu}\frac{Hx^2-(y-H)\left[(y-H)^2+H(y-H)+x^2\right]}{\left[x^2+(y-H)^2\right]^2}$$

For $Q_1(x,y)$

$$-\frac{16u_\delta RG}{3-4\nu}\frac{H^4+x^4-y^4+2Hy\left(y^2-H^2\right)+6x^2H(y-H)}{\left[x^2+(y-H)^2\right]^3}$$

For $Q_2(x,y)$

$$\frac{32u_\delta RG}{3-4\nu}x\frac{2H\left(H^2-x^2\right)-3yH^2+y\left(x^2+y^2\right)}{\left[x^2+(y-H)^2\right]^3}$$

For $q_1(x,y)$

$$\frac{16u_\delta RG}{3-4\nu}\left\{x\frac{x^2+y^2-H^2}{\left[x^2+(y-H)^2\right]^2}\right\}$$

For $q_2(x,y)$

$$\frac{16u_\delta RG}{3-4\nu}\frac{x^2(2H-y)-y(y-H)^2}{\left[x^2+(y-H)^2\right]^2}$$

Appendix VII. Summary of Derivation of Displacements due to Corrective Tractions for 3D Cavity

Corrective Tractions

$$\sigma_y^c\Big|_{y=0} = 2Gu_\varepsilon R^2\frac{3H^2-\left(x^2+z^2+H^2\right)}{\left(x^2+z^2+H^2\right)^{5/2}}$$

$$\tau_{yz}^c\Big|_{y=0} = 6Gu_\varepsilon R^2H\frac{z}{\left(x^2+z^2+H^2\right)^{5/2}}$$

$$\tau_{xy}^c\Big|_{y=0} = 6Gu_\varepsilon R^2H\frac{x}{\left(x^2+z^2+H^2\right)^{5/2}}$$

Stress Field due to Corrective Tractions

$$\sigma_y^c = 4Gy\frac{\partial^3\Psi^c}{\partial y^3} - 2G\frac{\partial^2\Psi^c}{\partial y^2}$$
$$\tau_{xy}^c = 4Gy\frac{\partial^3\Psi^c}{\partial x\partial y^2} + 2G\frac{\partial^2\Psi^c}{\partial x\partial y}$$
$$\tau_{yz}^c = 4Gy\frac{\partial^3\Psi^c}{\partial z\partial y^2} + 2G\frac{\partial^2\Psi^c}{\partial z\partial y}$$

Displacement Field due to Corrective Tractions

$$u_x^c = 2\frac{\partial}{\partial x}\left(y\frac{\partial\Psi^c}{\partial y}\right) + (3-4\nu)\frac{\partial\Psi^c}{\partial x}$$
$$u_z^c = 2\frac{\partial}{\partial z}\left(y\frac{\partial\Psi^c}{\partial y}\right) + (3-4\nu)\frac{\partial\Psi^c}{\partial z}$$
$$u_y^c = 2y\frac{\partial^2\Psi^c}{\partial y^2} - (3-4\nu)\frac{\partial\Psi^c}{\partial y}$$

Acknowledgments

The authors gratefully acknowledge the support provided by a research contract to Massachusetts Institute of Technology (MIT) and Universidad de Puerto Rico, Mayagüez and from the KKZ/CMA design-build team responsible for the Rio Piedras contract 7 of Tren Urbano for studying the performance tunnels constructed in Río Piedras, San Juan de Puerto Rico.

References

Boresi, A. P., and Chong, K. P. (1987). *Elasticity in engineering mechanics*, Elsevier Science, Amsterdam.

Brown, E. T., Bray, J. W., Ladanyi, B., and Hoek, E. (1983). "Ground response curves for rock tunnels." *J. Geotech. Engrg.*, 10.1061/(ASCE)0733-9410(1983)109:1(15), 15–39.

Gioda, G., and Swoboda, G. (1999). "Developments and applications of the numerical analysis of tunnels in continuous media." *Int. J. Numer. Anal. Methods Geomech.*, 23(13), 1393–1405.

González, C., and Sagaseta, C. (2001). "Patterns of soil deformations around tunnels. Application to the extension of Madrid Metro." *Comput. Geotech.*, 28(6–7), 445–468.

Kirsch, G. (1898). "Die theorie der elastizitaet und die bedeurfnisse der festigkeitslehre." *VDI Zeitschrift*, 42, 797–807 (in German).

Kovári, K. (1985). "The determination of characteristic lines from straight line nomograms." *Proc., Int. Conf. Numerical Methods in Geomechanics,* Balkema, Rotterdam, Netherlands, 1741–1748.

Loganathan, N., and Poulos, H. G. (1998). "Analytical prediction for tunneling-induced ground movements in clay." *J. Geotech. Geoenviron. Eng.*, 10.1061/(ASCE)1090-0241(1998)124:9(846), 846–856.

Mair, R. J., and Taylor, R. N. (1997). "Theme lecture: Bored tunnelling in the urban environment." *Proc., 14th Int. Conf. Soil Mechanics and Foundation Engineering*, Vol. 5, Balkema, Rotterdam, Netherlands, 2353–2385.

Mindlin, R. D., and Cheng, D. H. (1950). "Thermoelastic stress in the semi-infinite solid." *J. Appl. Phys.*, 21, 931–935.

Muskhelishvili, N. I. (1963). *Some basic problems of the mathematical theory of elasticity*, P. Noordhoff, Groningen, Netherlands.

Peck, R. B. (1969). "Deep excavations and tunnels in soft ground." *Proc., 7th Int. Conf. on Soil Mechanics and Foundation Engineering*, Sociedad Mexicana De Mecánica, Mexico City, 225–290.

Pinto, F. (1999). "Analytical methods to interpret ground deformations due to soft ground tunneling." S.M. thesis, Dept. of Civil and Environmental Engineering, Massachusetts Institute of Technology (MIT), Cambridge, MA.

Pinto, F., Zymnis, D., and Whittle, A. (2013). "Ground movements due to shallow tunnels in soft ground. II. Analytical interpretation and prediction." *J. Geotech. Geoenviron. Eng.*, 10.1061/(ASCE)GT.1943-5606.0000947, 04013041.

Potts, D. M., and Addenbrooke, T. I. (1997). "A structure's influence on tunnelling-induced ground movements." *Proc. Inst. Civ. Eng. Geotech. Eng.*, 125(2), 109–125.

Sagaseta, C. (1987). "Analysis of undrained soil deformation due to ground loss." *Geotechnique*, 37(3), 301–320.

Sagaseta, C. (1998). "Discussion on 'Surface settlements due to deformation of a tunnel in an elastic half plane' by A. Verruijt and J. R. Booker." *Geotechnique*, 48(5), 709–713.

Schmidt, B. (1969). "Settlements and ground movements associated with tunnelling in soils." Ph.D. thesis, Univ. of Illinois, Urbana-Champaign, IL.

Schürch, R., and Anagnostou, G. (2012). "The applicability of the ground response curve to tunneling problems that violate rotational symmetry." *Rock Mech. Rock Eng.*, 45(1), 1–10.

Sen, B. (1950). "Note on the stresses produced by nuclei of thermo-elastic strain in a semi-infinite elastic solid." *Q. Appl. Math.*, 8, 365–369.

Verruijt, A. (1996). "Complex variable solutions of elastic tunneling problems." *Rep. COB 96-04*, Geotechnical Laboratory, Delft Univ. of Technology, Delft, Netherlands.

Verruijt, A. (1997). "A complex variable solution for a deforming tunnel in an elastic half-plane." *Int. J. Numer. Anal. Methods Geomech.*, 21(2), 77–89.

Verruijt, A., and Booker, J. R. (1996). "Surface settlements due to deformation of a tunnel in an elastic half-plane." *Geotechnique*, 46(4), 753–756.

Yu, H. S., and Rowe, R. K. (1999). "Plasticity solutions for soil behaviour around contracting cavities and tunnels." *Int. J. Numer. Anal. Methods Geomech.*, 23(12), 1245–1279.

Zymnis, D., Chatzigiannelis, I., and Whittle, A. J. (2013). "Effect of anisotropy in ground movements caused by tunnelling." *Géotechnique*, 63(13), 1083–1102.